CHEMISTRY OF MATERIALS
Article

Chem. Mater. **2009,** *21,* 5349–5357 5349
DOI:10.1021/cm801323q

Structural Perturbations in Mesoporous Silica Microspheres Prepared Using Cationic Organosilanes.

Luc Beaudet, Roger Pitre, Lucie Robillard, and Louis Mercier*

Department of Chemistry and Biochemistry Laurentian University Sudbury, Ontario, Canada P3E 2C6

Received May 15, 2008. Revised Manuscript Received September 28, 2009

Mesoporous MSU silica microspheres were prepared by the hydrolysis of tetraethoxysilane (TEOS) in mildly acidic aqueous nonionic surfactant solutions in the presence of small amounts (molar percentage up to 1.25% with respect to TEOS) of cationic organotrialkoxysilanes (N-((trimethoxysilyl)propyl)-N,N,N-trimethylammonium chloride, N-((trimethoxysilyl)propyl)-N,N,N-tributylammonium chloride, and N-((trimethoxysilyl)propyl)- ammonium chloride). The incorporation of increasing amounts of cationic organotrialkoxysilanes results in the formation of microspherical MSU silica with increasingly perturbed mesopore structure (bimodal pore size distributions in the 30−120 Å range) and increasingly textural morphology. Functionalized derivatives of the microspheres were prepared by the substitution of TEOS with 3-mercaptopropyltrimethoxysilane (MPTMS) in the synthesis mixture. Gold ion adsorption studies were performed on the resulting microspheres, which showed that mildly perturbed microspheres, maintaining an adequate degree of uniformity in their mesopores, had optimal adsorption capacity and improved adsorption kinetics compared with both unperturbed and highly perturbed microspherical mesostructures.

Introduction

For more than a decade, mesostructure chemistry has provided an ever-growing tool chest of synthesis methodologies leading to the formation of nanoporous silica-based materials with tailored functionality and controlled nanostructural and morphological features.[1−20] These methods have been useful for the design of new materials for numerous applications, such as in environmental remediation,[1,7−9,14,16,17,19] catalysis,[1−6,12,15,18] and mineral processing,[20] to name but a few.

Functionalized mesostructures are now recognized as exceptional adsorbents, particularly with respect to metal ions.[7−16] By allowing the incorporating of high amounts of strategic functional groups (ligands) targeting specific metal ions or classes of metal ions, the open-framework pore network in these materials imparts unhindered access to all the ligand groups, resulting in materials with unsurpassed metal ion loading capacities. While other types of similarly functionalized materials (such as grafted silica gels, clays, and chelating polymer resins) also possess good metal ion adsorption capacity and specificity, access of the ions to the binding sites is typically incomplete because many of the binding sites are buried within the material matrix and are therefore inaccessible to the adsorbate ions.[7,9] This limitation is overcome by using structure-directing mesostructure synthesis strategies in the formation of tailored metal ions adsorbents. Although metal ion access to ligand sites is optimized in mesostructured systems, the diffusion of ions through mesopore channels was found to be in fact very slow (diffusion coefficients on the order of 10^{-14}−10^{-15} cm^2s^{-1}) and comparable to solid-state diffusion processes.[21] The adsorption kinetics of these materials is therefore controlled largely by the morphology of the mesostructure particles (viz., textural porosity, fundamental particle size, framework defects, etc.) rather than by the rate of ion ingress in the mesopore channels.[21]

*Corresponding author.

(1) Sayari, A.; Hamoudi, S. *Chem. Mater.* **2001**, *13*, 3151.
(2) Tanev, P. T.; Chibwe, M.; Pinnavaia, T. J. *Nature* **1994**, *368*, 321.
(3) Maschmeyer, T.; Rey, F.; Sankar, G.; Thomas, J. M. *Nature* **1995**, *378*, 159.
(4) Zhang, W.; Pinnavaia, T. J. *Catal. Lett.* **1996**, *38*, 261.
(5) Zhang, W.; Wang, J.; Tanev, P. T.; Pinnavaia, T. J. *Chem. Commun.* **1996**, 979.
(6) Zhang, W.; Froba, M.; Wang, J.; Tanev, P. T.; Wong, J.; Pinnavaia, T. J. *J. Am. Chem. Soc.* **1996**, *118*, 9164.
(7) Mercier, L.; Pinnavaia, T. *J. Adv. Mater.* **1997**, *9*, 500.
(8) Feng, X.; Fryxell, G. E.; Wang, L.-Q.; Kim, A. Y.; Liu, J.; Kemner, K. M. *Science* **1997**, *276*, 923.
(9) Mercier, L; Pinnavaia, T. J. *Environ. Sci. Technol.* **1998**, *32*, 2749.
(10) Lim, M. H.; Blanford, C. F.; Stein, A. *J. Am. Chem. Soc.* **1997**, *119*, 4090.
(11) Fowler, C. E.; Burkett, S. L.; Mann, S. J. *Chem. Commun.* **1997**, 1769.
(12) Van Rhijn, W. M.; DeVos, D. E.; Sels, B. F.; Bossaert, W. D.; Jacobs, P. A. *Chem. Commun.* **1998**, 317.
(13) Babonneau, F.; Leite, L.; Fontlupt, S. *J. Mater. Chem.* **1999**, *9*, 175.
(14) Brown, J.; Mercier, L.; Pinnavaia, T. J. *Chem. Commun.* **1999**, 69.
(15) Bossaert, W. D.; De Vos, D. E.; Van Rhijn, W. M.; Bullen, J.; Grobet, P. J.; Jacobs, P. A. *J. Catal.* **1999**, *182*, 156.
(16) Hossain, K. Z.; Mercier, L. *Adv. Mater.* **2002**, *14*, 1053.
(17) Bibby, A.; Mercier, L. *Green Chem.* **2003**, *5*, 15.
(18) Crudden, C. M.; Sateesh, M.; Lewis, R. *J. Am. Chem. Soc.* **2005**, *127*, 10045.
(19) Sawicki, R.; Mercier, L. *Environ. Sci. Technol.* **2006**, *40*, 1978.
(20) Abughusa, A.; Amaratunga, L.; Mercier, L. *Can. Metall. Q.* **2006**, *45*, 237.
(21) Bibby, A.; Mercier, L. *Chem. Mater.* **2002**, *14*, 1591.

Published on Web 10/27/2009

One notable class of silica-based mesostructure is that of MSU silica.[21−30] This mesostructure is prepared using polyethyleneoxide (PEO)-based nonionic surfactants under neutral or mildly acidic conditions. MSU silicas are characterized by their wormhole motif pore channel structure, and by the versatility of their synthesis process at forming functionalized derivatives with tailored physicochemical properties by one-step synthesis procedures by the co-condensation of organotrialkoxysilanes and tetraethoxysilane (TEOS).[24,27,28,30] The synthesis procedures of MSU silica can moreover be adapted to produce monodisperse microspheres of uniform size,[21,25,29,30] materials that have proven useful in providing insight about the diffusion mechanisms involved in the uptake of mercury ions inside the pore channels of thiol-modified mesostructures.[21] MSU microspheres are promising materials that may lead to the development of novel adsorbents and catalysts with well-defined structure, tailored functionality, and controlled adsorbate interaction properties.[21,30]

With the goal of generating novel anion-exchange materials, the functionalization of HMS, MCM-41, and SBA-15 mesostructures with cationic functional groups has been reported.[31a−c] In each of these works, either alkaline media (encountered in HMS and MCM-41 syntheses) or highly acidic media (typical in SBA-15 syntheses) were employed in order to in MSU-type mesostructures, in which neutral to mildly acidic hydrolysis environments are used for their preparation.[21−30] The goal of the present study is to investigate the possibility of incorporating cationic organosilane moieties inside MSU silica microspheres, and to study the influence of such functions on the formation and structure of the mesostructures. Toward this end, three cationic moieties were incorporated in the structure of MSU silica microspheres by using appropriately functionalized trialkoxysilane derivatives: propyltrimethylammonium chloride (—CH_2-$CH_2CH_2NMe_3^+Cl^-$, $PrTMA^+$), propyltributylammonium chloride (—$CH_2CH_2CH_2NBu_3^+Cl^-$, $PrTBA^+$), and propylammonium chloride ($CH_2CH_2CH_2NH_3^+Cl^-$, $PrNH_3^+$). The preparation of functional derivatives of these microspheres by the subsititution of TEOS with an organosilane (3-mercaptopropyltrimethoxysilane, MPTMS, in the present case) in the synthesis was also undertaken, and the adsorption properties (adsorption capacity and kinetics) of the resulting materials characterized using $AuCl_4^-$ as a test subject.[32,33]

Experimental Section

Chemicals. All chemicals were obtained from Aldrich Chemicals and used without further purification.

Mesostructure Synthesis. The mesostructures were prepared following an adapted version of the MSU microsphere synthesis procedure initially introduced by Boissière et al.[25,26] In a typical preparation, a mixture of tetraethoxyxilane (TEOS, $(1 - X) \times 2.16\times10^{-2}$ mol) and organotrialkoxysilane ($X\times2.16\times 10^{-2}$ mol), where X = 0.0025, 0.0050, 0.0075, 0.0100, and 0.0125) was added to 100 mL of a stirred aqueous solution of Igepal CA-720 ($C_8H_{17}{}^-C_6H_5-(OCH_2CH_2)_{10}OH$, 2.69×10^{-3} mol) acidified with 5 mL of HCl (0.20 M). The organosilanes used were N-((trimethoxysilyl)propyl)-N,N,N-trimethylammonium chloride ($PrTMA^+$-TMS, 50% in methanol), N-((trimethoxysilyl)propyl)-N,N,N-trimethylammonium chloride ($PrTMA^+$-TMS, 50% in methanol), and 3-aminopropyltriethoxysilane (APS-TMS). The synthesis parameter X corresponds to the mole fraction of organosilane with respect to total silane (TEOS + organosilane, 2.16×10^{-2} mol). When 3-aminopropyltriethoxysilane (APS-TMS) was used, an equimolar amount of HCl was added to the mixture in addition to the 5 mL of HCl 0.20 M to convert the aminopropyltrimethoxysilane into the ammonium conjugate acid form (viz., N-((triethoxysilyl)propyl)ammonium chloride, $PrNH_3^+$-TES). The mixtures were stirred for 1 h to yield clear solutions and transferred to a thermostatted water bath set at 30 °C. NaF (0.03825 g) was added to the solution, which was quickly stirred then left to sit undisturbed for 24 h to allow precipitation of the product. The resulting material was freeze-dried, and the framework bound surfactant removed by Soxhlet extraction over ethanol for 24 h. The materials were named in accordance with to the amount of their incorporated functional groups and the surfactant used to form the materials. The mesostructures consist of an MSU-2 structure as it was assembled using the alkyl(aryl)poly(ethylene oxide) surfactant IgepalCA-720[22] and were hereafter designated $PrTMA^+$-X-MSU-2, $PrTBA^+$-X-MSU-2, and $PrNH_3^+$-X-MSU-2, where X corresponds to the percentage of the cationic functional group incorporated during the synthesis (with respect to the total silane used in the synthesis).

Functionalized derivatives of the aforementioned mesostructures were prepared using the same procedures described above, with the exception that the molar quantity of TEOS used in the synthesis was decreased by 5% and replaced by a corresponding molar quantity of 3-mercaptopropyltrimethoxysilane (MPTMS). The resulting thiol-functionalized nanostructures were hereafter designated MP-$PrTMA^+$-X-MSU-2, MP-$PrTBA^+$-X-MSU-2, and MP-$PrNH_3^+$-X-MSU-2, in accordance with the nomenclature system described above.

Mesostructure Characterization. Powder X-ray diffraction patterns were measured on a Rigaku Rotaflex diffractometer equipped with a rotating anode and using Cu Kα radiation (Ontario Geoscience Laboratories, Sudbury, Ontario, Canada). The lattice spacings (d) of the materials were calculated by

(22) Bagshaw, S. A.; Prouzet, E.; Pinnavaia, T. J. *Science* **1995**, *269*, 1242.
(23) Prouzet, E.; Pinnavaia, T. J. *Angew. Chem., Int. Ed., Engl.* **1997**, *36*, 516.
(24) Richer, R.; Mercier, L. *Chem. Commun.* **1998**, 1775.
(25) Boissière, C.; van der Lee, A.; El Mansouri, A.; Larbot, A.; Prouzet, E. *Chem Commun.* **1999**, 2047.
(26) Boissière, C.; Larbot, A.; van der Lee, A.; Kooyman, P. J.; Prouzet, E. *Chem. Mater.* **2000**, *12*, 2902.
(27) Brown, J; Richer, R.; Mercier, L. *Microporous Mesoporous Mater.* **2000**, *37*, 41.
(28) Richer, R.; Mercier, L. *Chem. Mater.* **2001**, *13*, 2999.
(29) Boissière, C.; Larbot, A.; Bourgaux, C.; Prouzet, E.; Bunton, C. A. *Chem. Mater.* **2001**, *13*, 3580.
(30) Beaudet, L.; Hossain, K. Z.; Mercier, L. *Chem. Mater.* **2003**, *15*, 327.
(31) (a) Lee, B.; Bao, L.-L.; In, H.-J.; Dai, S.; Hagaman, E. W.; Lin, J. S. *Langmuir* **2003**, *19*, 4246.(b) Walcarius, A.; Ganesan, V. **2006**, *22*, 469. (c) Zhou, L.-H.; Zhang, L.-Z.; Hu, J.; Zhao, X.-G.; Liu, H.-L. *Acta Phys.-Chim. Sin.* **2007**, *23*, 620.
(32) Guari, Y; Thieuleux, C.; Mehdi, A.; Reyé, C.; Corriu, R. J. P.; Gomez-Gallardo, S.; Philippot, K.; Chaudret, B.; Dutartre, R. *Chem. Commun.* **2001**, 1374.
(33) Lam, K. F.; Yeung, K. L.; McKay, G. *J. Phys. Chem.* **2006**, *110*, 2187.

applying Bragg's Law to the maximum in the diffraction peaks observed in the patterns ($d = 1.54$ Å$/2\sin\theta$).

N_2 adsorption isotherms of the adsorbents were measured at −196 °C on a Micromeritics ASAP 2010 sorptometer. Prior to measurement, all samples were outgassed at 110 °C at 10^{-6} mm Hg. BET surface areas were measured from the linear part of the BET plot ($0.05 < P/P_0 < 0.25$). Mesopore volumes were assumed to be equal to the liquid volume of adsorbed nitrogen below $P/P_0 = 0.7$. Pore size distributions were calculated using the Broekhoff-deBoer (BdB) method.[34] The wall thicknesses of the mesostructures were obtained by subtracting the pore diameters from the d spacings.

The scanning electron microscopy (SEM) images of the adsorbents were obtained by a frame integration of 30 frames on a Zeiss EVO-50 scanning electron microscope under an accelerating voltage of 1.33 kV and a beam current of 4pA (Ontario Geoscience Laboratory, Sudbury). The diameters of the microspherical particles were measured from the SEM images using ImageJ 1.34s software (http://rsb.info.nih.gov/ij/).

Adsorption of $AuCl_4^-$ by Mesostructures. Adsorption isotherms for MP-MSU-2, MP-PrNMe$_3^+$-0.25-MSU-2, MP-PrNMe$_3^+$-0.50-MSU-2, MP-PrNMe$_3^+$-0.75-MSU-2, and MP-PrNMe$_3^+$-1.00-MSU-2 were obtained by stirring 5 mg samples of each material in 50 mL of $(NH_4)AuCl_4$ solutions with concentrations in the range 5−50 mg Au/L for 24 h. The mixtures were then filtered and the filtrate analyzed for Au by flame AAS. The amount of Au adsorbed by the materials were determined by subtracting the amount of Au remaining in the solution from the initial amount of Au in the stock solutions.

The kinetics of the Au adsorption by the mesostructures were also measured by stirring 2 mg samples of each MP-functionalized mesostructure in 20 mL of $AuCl_4^-$ solution (15 mg Au/L) for set time periods (ranging from 1 to 120 min). The mixtures were then rapidly filtered and the Au concentration remaining in the solution was measured by flame AAS. The amount of Au taken up by the materials at various exposure times was determined by subtracting the amount of Au remaining in the solution from the initial amount of Au in the stock solutions.

Results and Discussion

Inhibition of Formation and Structural Perturbation of MSU Silica. It became quickly apparent at the outset of these studies that introducing even very small amounts of cationic organosilanes in the synthesis mixtures of MSU silica (specifically, greater than 1.25 mol % with respect to total silane content) resulted in complete absence of product formation. The addition of small amounts of cationic organosilanes (under 1.25 mol % with respect to total silane), on the other hand, results in the formation of MSU silica, although with significant alterations in both the nanoscale structure and particle morphology of the materials. The results of this work suggest that the root cause of this phenomenon is linked to the hydrophilic nature of the cationic organosilanes. The following discussion proposes a plausible mechanistic account of these structural perturbations, after which experimental evidence supporting the proposed mechanism will be presented in greater detail. Lastly, the metal ion adsorption behavior (using $AuCl_4$ as a test subject) of functionalized derivatives of the perturbed mesostructures will be presented and discussed in relation to their structural characteristics.

Proposed Mechanism of Formation of Perturbed MSU Silica. Previous mechanistic investigations on the formation of MSU mesostructures,[29] using tetraethoxysilane (TEOS) as a source of silica, have found that these materials are prepared by (i) the hydrolytic formation of oligomeric silica precursors in the amphiphilic "corona" of the surfactant micelles (viz., a region between the hydrophobic "core" of the micelles and the bulk water phase), followed by (ii) the cross-linking of the precursors within the corona with that surrounding other micelles, precipitating the final product. An abbreviated depiction of this formation mechanism is shown in Figure 1 (left diagram). This process was subsequently shown to be amenable for the preparation of organosilane-functionalized derivatives of microspherical MSU structures.[30]

In general, the addition of reasonable amounts of organosilanes in MSU synthesis (under ∼20% organosilane/total Si ratios) results in the formation of mesostructures with essentially identical mesoscale order and pore channel uniformity as their nonfunctionalized pure silica analogs.[30] Such consistency in structural order is generally considered to result from the favorable interaction of most types of organosilane functions (such as alkyl, mercaptopropyl, aromatic, etc.) with the structure-directing micelles, allowing the cross-linking of TEOS and organosilane to happen at the surfactant:water interface without the occlusion of the organic functions in the pore walls. The cationic organosilanes used in the present investigation, on the other hand, have substantial more affinity toward water than they do with the hydrophobic environment of the micelles. Thus, when a sufficiently large amount of cationic organosilane is added to the synthesis mixture of MSU-silica (above 1.0% with respect to total silane content, as evidence will show further), oligomeric silica precursors bearing cationic functions are formed. As depicted in Figure 1 (middle diagram), these functions cause the precursors to move into the aqueous phase of the micelle solution rather than to assemble at the micelle interface, resulting in the absence of mesostructure formation.

When very small amounts of cationic organosilanes (less than ∼1.0% with respect to total silane content) are added to the reaction mixture, however, formation of product is observed. Under these conditions, it can be inferred that the cationic charges borne by the silica precursors are sufficiently dispersed as to not entirely prevent mesostructure formation. As evidenced by X-ray diffraction, porosimetry, and electron microscopy (details of these analyses will be presented in the Nanostructural Transformations in Perturbed MSU Silica and Morphological Transformations subsections below), the materials thus formed still exhibit the general physical characteristics of MSU silica, although with increasing perturbations in their nanoscale structures and in their particle morphology.

As shown in Figure 1 (right diagram), it is proposed that the cationic group-bearing silica precursors tend to

(34) Broekhoff, J. C. P.; de Boer, J. H. *J. Catal.* **1968**, *10*, 377.

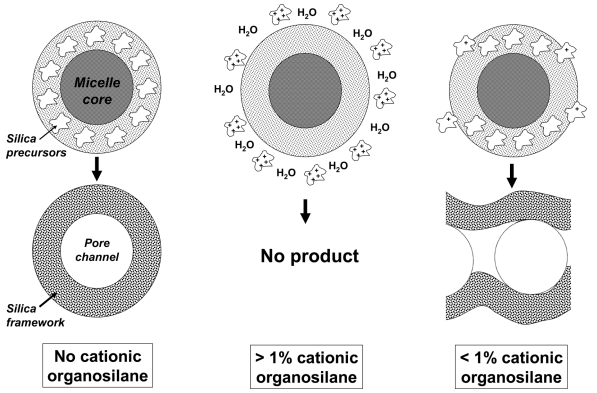

Figure 1. Depiction of proposed formation mechanism of perturbed MSU silica mesostructures. Left diagram: In the absence of cationic organosilanes, uncharged oligomeric silica precursors are formed, which subsequently cross-link into surfactant-assembled MSU mesostructures with uniform nanoporosity. Middle diagram: The addition of significant amounts of cationic organosilanes (>1% of the total silane content) forms charged silica precursors which migrate away from the micelle−water interface and into the bulk water phase, inhibiting mesostructure formation. Right diagram: The addition of small amounts of cationic organosilane (<1% of the total silane content) forms a restricted number of slightly charged precursors that retain some affinity with the micelle interface, but tend to migrate toward the aqueous phase and form perturbed derivatives of MSU silica.

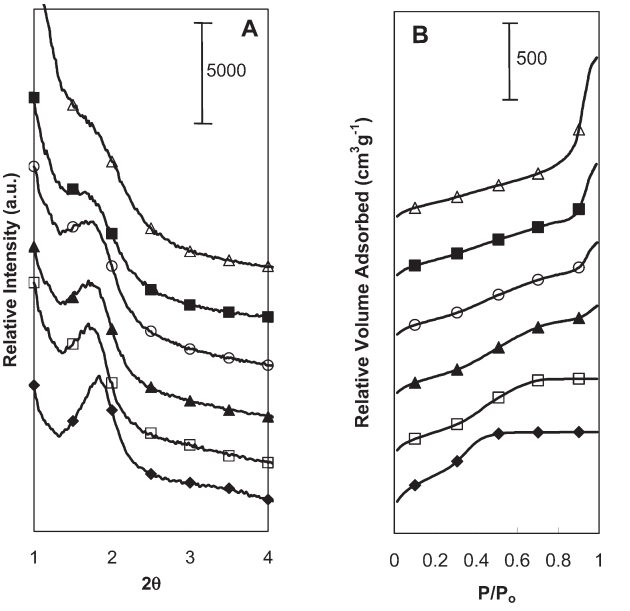

Figure 2. Representative powder XRD patterns (A) and N_2 adsorption isotherms (B) for $PrTMA^+$-MSU-2 microspheres prepared using different functional group loadings: (♦) 0.00%, (□) 0.25%, (▲) 0.50%, (○) 0.75%, (■) 1.00%, and (△) 1.25%. The pattern baselines were offset for visual clarity. The symbols on the curves are meant for identification, and are not data points. The desorption curves in isotherms in (B) were not shown in the interest of clarity. (For an example of a complete isotherm, see the Supporting Information).

migrate away from the micelle−water interface. The relative scarcity of cationic groups in reaction mixture composed of very low amounts of cationic groups, however, limits the number of precursors that bear cationic functions so as to nonetheless allow the formation of a silica framework at the micelle interface. The presence of cationic oligomers, however, results in the formation of structures that become increasingly structurally perturbed as a function of both cationic group content and the natures of the cationic group itself.

Comparison with Previously Reported $PrTMA^+$- and $PrTBA^+$-Functionalized Mesostructures. In contrast with what is observed in the present work, Lee et al. reported various successful one-step synthesis surfactant-assembly procedures resulting in mesoporous silica structures containing $PrTMA^+$ and $PrTBA^+$ moieties with loadings of 15% with respect to the framework-forming silica precursors.[31] These materials were prepared using alkylamine surfactants (such as in the synthesis of HMS silica), using alkylammonium surfactants with NaOH (such as in the preparation of MCM-41), and using nonionic surfactants (Pluronic P-123) under highly acidic media (such as in the formation of SBA-15). HMS and MCM-41 synthesis both involve base-mediated hydrolysis of the framework-forming silane precursors, whose kinetics are considerably more rapid than those of the mildly acidic fluoride-mediated hydrolysis method studied in the present work. The incorporation of significant amount of cationic functional groups thus occurs because the framework cross-links at the micelle interface before the charge-bearing precursors migrate into the aqueous phase. A similar argument can be invoked to explain the incorporation of cationic groups using the SBA-15 synthesis procedure, wherein the extremely high acidic conditions also promote rapid hydrolysis and framework cross-linking. Thus, the neutral or mildly acidic hydrolysis conditions used in the synthesis of MSU mesostructures results in products whose structures (both at the nanoscale and at the microscale) become significantly affected by the subtle solution effects encountered by the framework-forming silica precursors.

Nanostructural Transformations in Perturbed MSU Silica. The XRD patterns of the materials (Figure 2A) were indicative of the random wormhole motif structure expected in MSU silica, featuring broad diffraction peaks centered at 2θ angles near 2°.[21−30] The intensity and breadth of the diffraction peaks reduced slightly as the percentage of cationic organosilane increased in the samples, although the pattern intensities did not diminish significantly up to compositions of 1% cationic organosilane (Figure 2A). Only at 1.25% loading did the peaks begin to disappear, at the point where product formation begins to be compromised. A comparison between the XRD patterns of the $PrTMA^+$-functionalized materials and that of the corresponding $PrTBA^+$-functionalized series reveals somewhat improved quality of the patterns for the latter. This may be attributed to the increased affinity of the tetrabutylammonium headgroup of $PrTBA^+$ moiety toward the assembly surfactant compared to that of $PrTMA^+$, resulting in improved order in the mesostructure. The addition of cationic organosilanes in MSU silica synthesis did not have any significant effect of the materials' lattice spacings, which remained about 50 Å in all cases (Table 1).

The perturbing effects of the cationic organosilanes is most clearly observed in the N_2 adsorption isotherms of the materials (Figure 2B, full isotherms including desorption

Table 1. Structural Characteristics of MSU-2 and Cationic Organosilane-Modified Derivatives

material designation	BET surface area (m^2g^{-1})	mesopore volume (cm^3g^{-1})	pore diameter (Å)	lattice spacing (Å)	particle size (μm)
MSU-2	1159	1.04	37	49.0	3.5 ± 0.6
$PrTMA^+$-0.25-MSU-2	832	0.81		50.7	2.4 ± 0.4
$PrTMA^+$-0.50-MSU-2	760	0.84		49.6	2.0 ± 0.3
$PrTMA^+$-0.75-MSU-2	672	0.67		51.9	1.5 ± 0.2
$PrTMA^+$-1.00-MSU-2	598	0.57			
$PrTMA^+$-1.25-MSU-2	597	0.63			
$PrTBA^+$-0.25-MSU-2	930	0.97	41	50.1	2.8 ± 0.4
$PrTBA^+$-0.50-MSU-2	846	0.90	41	48.5	2.7 ± 0.4
$PrTBA^+$-0.75-MSU-2	724	0.77		50.1	2.0 ± 0.3
$PrTBA^+$-1.00-MSU-2	711	0.70		52.5	1.7 ± 0.3
$PrTBA^+$-1.25-MSU-2	627	0.64		50.7	1.4 ± 0.2
$PrNH_3^+$-0.25-MSU-2	1218	1.08	37	49.0	2.5 ± 0.5
$PrNH_3^+$-0.50-MSU-2	1036	1.00	39	49.0	2.2 ± 0.5
$PrNH_3^+$-0.75-MSU-2	961	0.91	39	51.9	1.9 ± 0.3
$PrNH_3^+$-1.00-MSU-2	848	0.77	37	50.7	1.7 ± 0.3
$PrNH_3^+$-1.25-MSU-2	870	0.71	34	50.1	

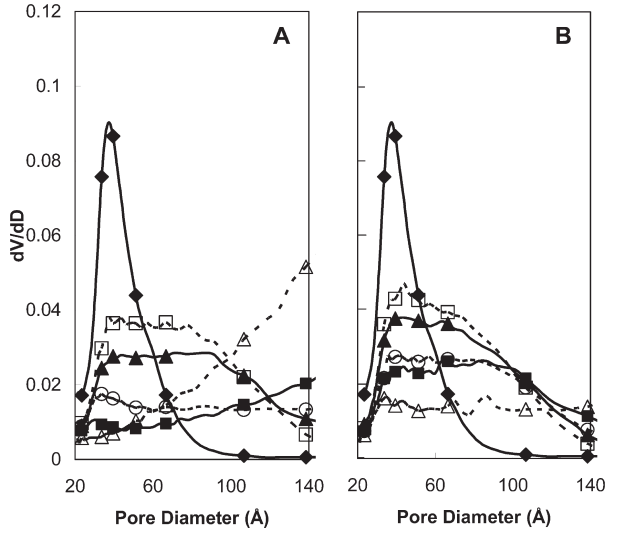

Figure 3. Pore-size distributions for (A) $PrTMA^+$-MSU-2 and (B) $PrTBA^+$-MSU-2 microspheres prepared using different functional group loadings: (♦) 0.00%, (□) 0.25%, (▲) 0.50%, (○) 0.75%, (■) 1.00%, and (Δ) 1.25%. The symbols on the curves are meant for identification, and are not data points.

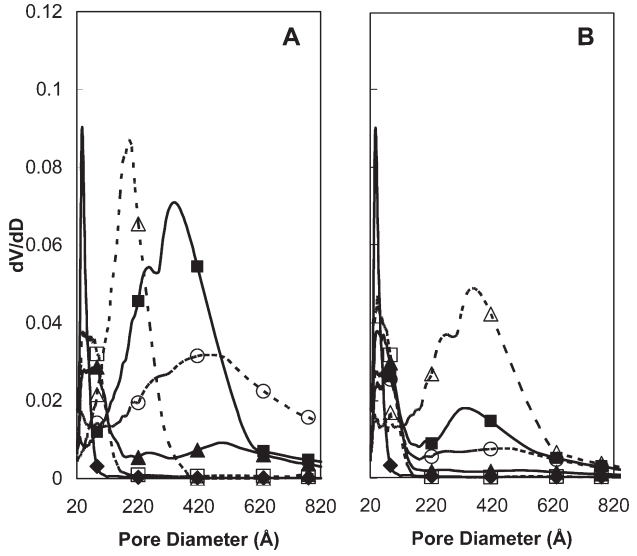

Figure 4. Wider scale pore-size distributions for (A) $PrTMA^+$-MSU-2 and (B) $PrTBA^+$-MSU-2 microspheres prepared using different functional group loadings: (♦) 0.00%, (□) 0.25%, (▲) 0.50%, (○) 0.75%, (■) 1.00%, and (Δ) 1.25%. The symbols on the curves are meant for identification, and are not data points.

branches are shown in Supporting Information (SI) Figures S1−S6), and in their corresponding pore size distributions (Figures 3 and 4). The inflection in the N_2 adsorption for the mesostructures, normally observed between P/P_0 values between 0.3 and 0.4 for nonfunctional MSU silica (Figure 2), is found to broaden and shift to higher values of P/P_0 upon increasing cationic organosilane loading (Figure 2B). Moreover, at loading of 0.5% and higher, an increasingly prominent inflection approaching P/P_0 of 1.0 is observed in the materials (Figure 2B). These results denote a systematic decrease in the order and uniformity of the pore channels and a concomitant increase in textural porosity corresponding to the increased loadings of cationic organosilane groups. While the mesostructures prepared with cationic organosilane loadings of 0.5% or less exhibited the hysteresis loops (rejoining the adsorption curves at P/P_0 0.4−0.5) typically observed in mesoporous materials (Figures S1−S3), the shifting of these loops to higher P/P_0 ranges in the more highly loaded materials (approaching 1.0 in the case of 1.0% and 1.25 loadings, Figure S4−S6) denotes significant perturbation and loss of uniformity in the mesopore channels. These structural distortions are consistent with the proposed mechanism previously discussed (Figure 1).

The pore size distributions of the materials reveal the gradual disappearance of the uniform 37−40 Å mesopores in the materials (Figure 3), while their textural porosity (above 200 Å) increased (Figure 4). The reduction in mesoporosity of the samples is associated with concomitant reduction in their specific surface area and uniform mesopore volumes (Table 1). In the case of mesostructures prepared using $PrTMA^+$ and $PrTBA^+$, the disappearance of the 37−40 Å uniform mesopores was associated with the emergence of a broader envelope of size distributions in the 30−120 Å range (Figure 3A and 3B). The general appearance of these broad sets of pore size distributions suggests that bimodal mesoporosity results from the addition of cationic organosilanes in the synthesis of the mesostructures. Gaussian deconvolution of the pore size distributions corroborated this

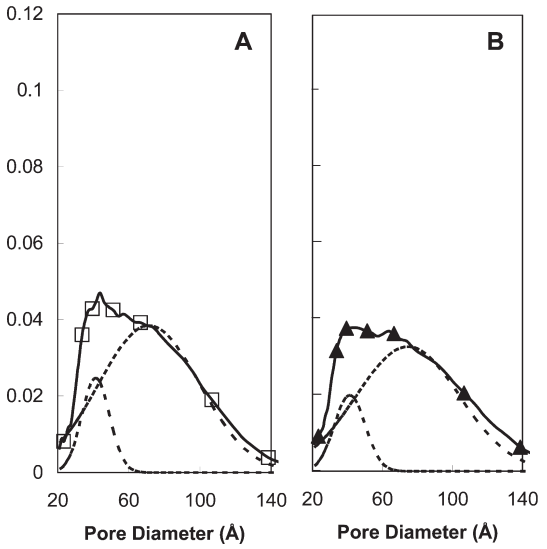

Figure 5. Pore-size distributions for (A) $PrTBA^+$-0.25-MSU-2 and (B) $PrTBA^+$-0.50-MSU-2 mesostructures and their respective Gaussian line shape analyses (dotted lines). $R^2 = 0.99149$ for the deconvolution of curve (A) and $R^2 = 0.98952$ for that of curve (B).

observation, showing accurate fitting of the data ($R^2 \sim 0.99$) using double Gaussian line shape analysis (Figure 5). While the first peak resolved from the deconvolution analysis was characteristic of the "normal" uniform mesoporosity (centered at ~40 Å, Figure 5), the second peak showed a broader pore size distribution centered at ~75 Å.

It can be speculated that this second pore size distribution is the result of the merger of multiple mesopores into one larger combined pore channel, as depicted in Figure 6. This pore merger likely results from absence of wall formation where cationic oligomers were present prior to cross-linking, the latter migrating into the aqueous phase and leaving openings where walls would normally have formed (see Figure 1, right diagram). Although the merging of pore channels results in major changes in the nanopore structure of the materials, the periodic wormhole structure of the mesostructures (as perceived by the XRD diffraction patterns) is largely retained due to the presence of "vestigial" pore channels such as depicted in Figure 6B (which are hereafter denoted as *phantom pore channels*). This hypothesis is plausible to explain why the observed intensity and breadth of the materials' XRD patterns remain largely unchanged (at least for cationic organosilane compositions below 1%), while their nanopore channels become significantly perturbed. This explanation, moreover, is consistent with the proposed mechanism discussed previously (Figure 1).

Morphological Transformations. The SEM images of the mesostructures revealed that the materials generally retained monodisperse spherical morphology with cationic organosilane compositions up to 1.0% (Figures 7 and 8). At higher content of cationic moieties, the materials appear instead as highly textural irregular-shaped particles. Whereas the nonfunctionalized MSU microspheres appear as smooth particles, the addition of cationic organosilane functionalities caused the microspheres to

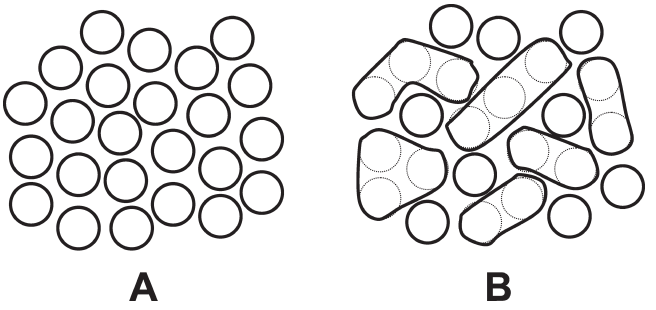

Figure 6. Depiction of cross-sectional pore channel structure of (A) MSU silica with uniform-diameter mesopores, and that speculated for (B) MSU silica prepared with cationic organosilane functional groups in which pore channels are merged together. The dotted circles in (B) denote the remnant "phantom" porosity in the perturbed mesostructures.

adopt increasingly pocked and textured morphology (Figure 8). The increasing degree of texture observed in the materials is reflected by the increasing evolution of textural porosity in the 200−700 Å (20−70 nm) range (Figure 5) resulting from the increased structural perturbations in these systems.

The particle sizes of the microspheres also systematically decreased as a function of the amount of cationic organosilane in the mesostructures (Figure 9, Table 1). The presence of cationic organosilanes in the synthesis of MSU silica inhibits the growth rate of the microspheres, resulting in a faster relative rate of particle nucleation. The net result is, therefore, the formation of a greater number of particles of smaller size.

When comparing the particle sizes of the $PrTMA^+$- and $PrTBA^+$-functionalized mesostructures (Figure 9A and 9B, Table 1), it is observed that the $PrTBA^+$-functionalized materials have larger particle sizes than the corresponding $PrTMA^+$ series. This may be attributed to the increased hydrophobicity of $PrTBA^+$ moieties, which slightly offsets the inhibiting charge effect in the rate of particle growth. The spherical morphology of the materials, moreover, is preserved to higher functional group loading in the $PrTBA^+$-functionalized materials than in the $PrTMA^+$ series (e.g., a few spherical particles can be seen in the SEM images of $PrTBA^+$-1.25-MSU-2), an observation that may be again ascribed to the greater hydrophobicity of the $PrTBA^+$ moiety.

Nano- and Microstructural Characteristics of Functionalized Mesostructures. The thiol-functionalized mesostructures obtained by substituting 5% of the TEOS with MPTMS in the synthesis mixture (viz., the MP-$PrTMA^+$-*X*-MSU-2, MP-$PrTBA^+$-*X*-MSU-2, and MP-$PrNH_3^+$-*X*-MSU-2 series) all had essentially identical nanoscale and microscale features as that of their nonfunctionalized counterparts (except for slightly smaller pore diameters due to the presence of the organic functions inside the pore channels). The incorporation of functional groups such as mercaptopropyl in the synthesis of MSU microspheres and their perturbed derivatives thus has minimal influence on the characteristics of the obtained mesostructures.

Adsorption Properties of Perturbed Mesoporous Microspheres. In all cases, the thiol-functionalized mesostructures

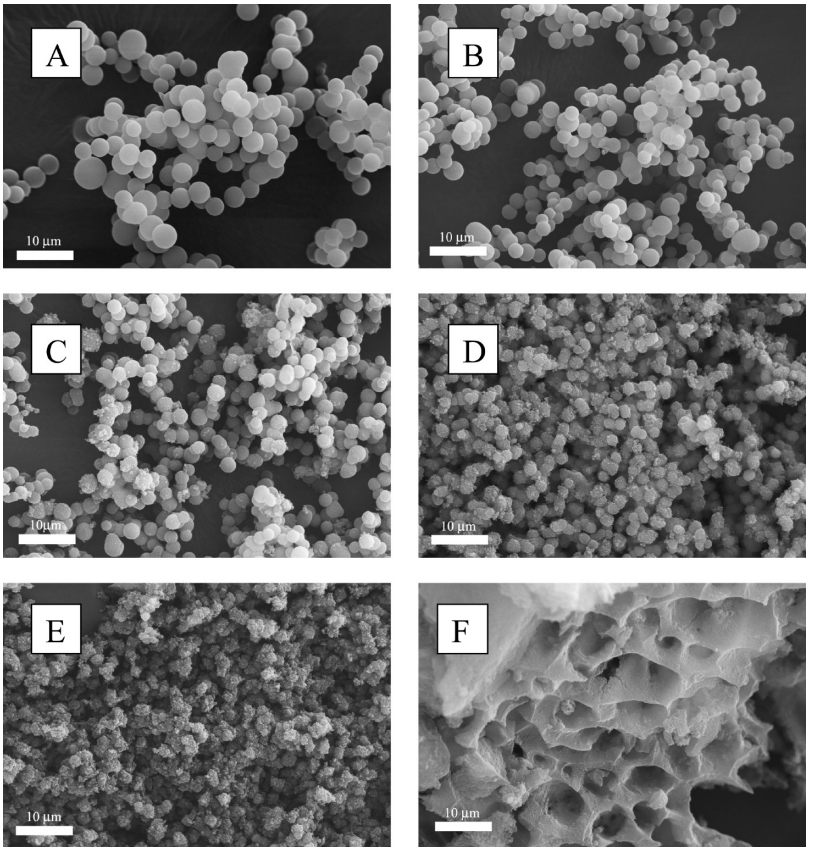

Figure 7. Lower resolution SEM images of (A) MSU-2, (B) $PrNH_3^+$-0.25-MSU-2, (C) $PrNH_3^+$-0.50-MSU-2, (D) $PrNH_3^+$-0.75-MSU-2, (E) $PrNH_3^+$-1.00-MSU-2, (F) $PrNH_3^+$-1.25-MSU-2.

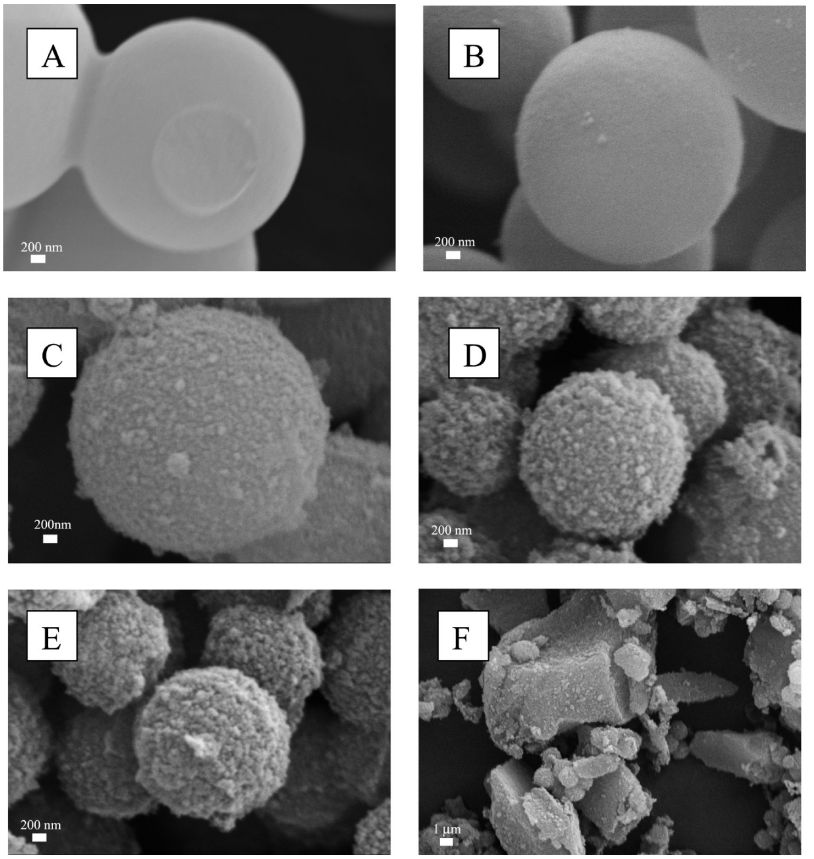

Figure 8. Higher resolution SEM images of (A) MSU-2, (B) $PrTBA^+$-0.25-MSU-2, (C) $PrTBA^+$-0.50-MSU-2, (D) $PrTBA^+$-0.75-MSU-2, (E) $PrTBA^+$-1.00-MSU-2, (F) $PrTBA^+$-1.25-MSU-2.

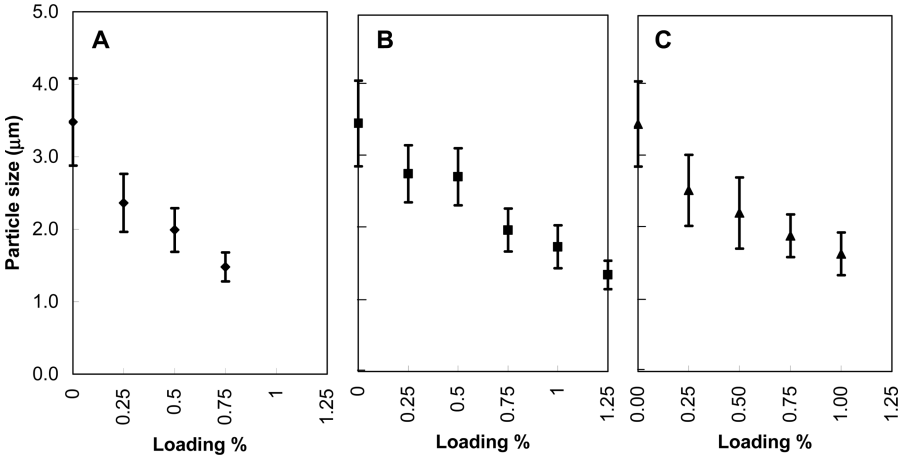

Figure 9. Particle size as a function of loading percentage of (A) $PrTMA^+$, (B) $PrTBA^+$, and (C) $PrNH_3^+$. The error bars represent the standard deviations of particle diameters within each representative sample.

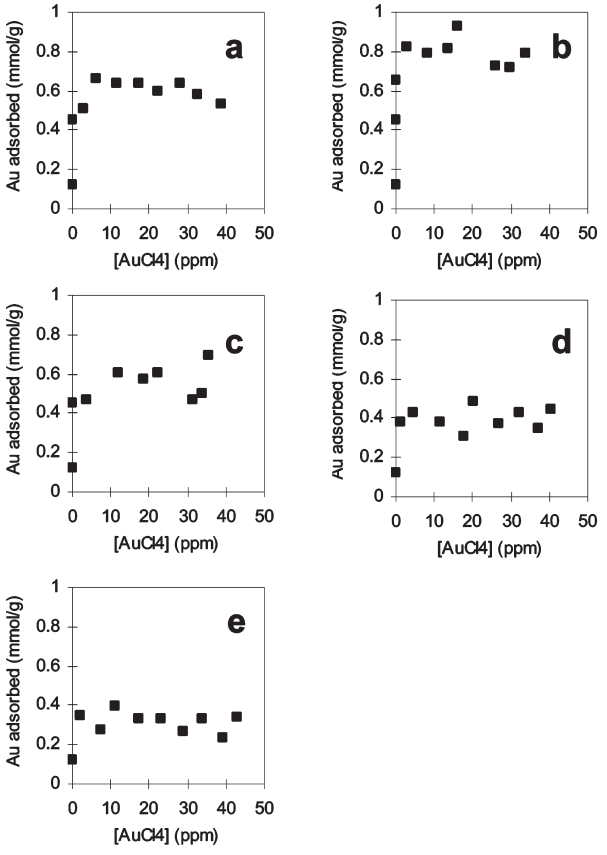

Figure 10. $AuCl_4^-$ adsorption isotherms for (a) MP-MSU-2, (b) MP-$PrNMe_3^+$-0.25-MSU-2, (c) MP-$PrNMe_3^+$-0.50-MSU-2, (d) MP-$PrNMe_3^+$-0.75-MSU-2, and (e) MP-$PrNMe_3^+$-1.00-MSU-2.

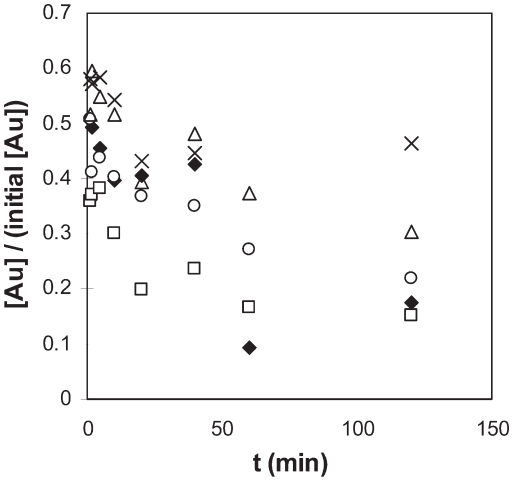

Figure 11. Kinetic profile of Au adsorption by nanoporous microspheres, represented as the fraction of $AuCl_4^-$ adsorbed ($[Au]_t/[Au]_0$) as a function of time by (♦) MP-MSU-2, (□) MP-$PrNMe_3^+$-0.25-MSU-2, (○) MP-$PrNMe_3^+$-0.50-MSU-2, (Δ) MP-$PrNMe_3^+$-0.75-MSU-2, and (X) MP-$PrNMe_3^+$-1.00-MSU-2. In each experiment, 2 mg of adsorbent was stirred in 20 mL of 15 mg L^{-1} $(NH_4)AuCl_4$ aqueous solution.

were very effective in adsorbing Au ions, reaching saturation levels at low residual Au concentration (Figure 10). Different mesostructures, however, achieved vastly different adsorption capacities according to the extent of their structural perturbation. The structurally unperturbed MP-MSU-2 mesostructure, for instance, was found to have an adsorption capacity for $AuCl_4^-$ of 0.61 mmol/g (Figure 10a), which represents the binding of the metal ions to approximately 75% of the thiol groups in the mesostructure (determined as 0.80 mmol/g based on the composition of the material), assuming a 1:1 complexation between the ligand and metal. On the other hand, the adsorption capacity of the MP-$PrNMe_3^+$-0.25-MSU-2 mesostructure was elevated to 0.80 mmol/g (Figure 10b), indicating 100% access to the thiol ligands by the metal. These results suggest that the textural porosity present in the mildly perturbed MP-$PrNMe_3^+$-0.25-MSU-2 provides total access of the metal ions to the thiol groups in the pore channels. The incomplete access of the $AuCl_4^-$ ions to the thiol moieties in MP-MSU, on the other hand, may be attributed to the absence of textural porosity in this mesostructure's particles, inhibiting access to some of the thiol groups in the material (perhaps those located deep within the particle). The adsorption capacities of $AuCl_4^-$ for the highly structurally perturbed mesostructures (MP-$PrNMe_3^+$-0.50-MSU-2, MP-$PrNMe_3^+$-0.75-MSU-2, and MP-$PrNMe_3^+$-1.00-MSU-2) were found to diminish systematically as a function of their degree of structural perturbation (with values of 0.56, 0.40, and 0.32 mmol/g for MP-$PrNMe_3^+$-0.50-MSU-2, MP-$PrNMe_3^+$-0.75-MSU-2, and MP-$PrNMe_3^+$-1.00-MSU-2,

respectively, see Figure 10c−e). Despite the increasing degree of textural porosity present in these materials, the reduction of adsorption capacity in the latter can be attributed to the increasing degree of disorder in their mesopore channels, thereby systematically impeding metal ion access to the thiol ligands. These observations are consistent with prior research comparing Hg^{2+} adsorption by thiol-functionalized mesostructured silica with similarly derivatized silica gel, which likewise reported impeded ligand access in disordered silica gel networks, and (near) complete access to the ligands in mesostructures with uniform mesopores.[7,9]

The preliminary diffusion studies conducted also found that MP-PrNMe_3^+-0.25-MSU-2, which possessed optimal adsorption capacity toward Au ions, also exhibited the most rapid sorption kinetics in comparison to either MP-MSU-2 or the more perturbed mesostructures, especially in the 0−60 min time scale (Figure 11). These results once again are in accordance with the proposition that the presence of textural porosity in mesostructure particles, coupled with adequately uniform nanoscale porosity, promoted optimal sorption properties in tailored nanostructured adsorbents (both in terms of affinity and kinetics).

Conclusions

This work has revealed numerous interesting effects of adding cationic functional groups in MSU-type mesoporous silica, particularly regarding their influence of the pore structure and morphology of the mesostructures, and also provides new insights about the various solution effects that come into play during the assembly of mesostructures using nonionic surfactants under mild acidic conditions.

From a technological perspective, these materials offer some interesting prospects for applications in areas such as adsorption and catalysis. As demonstrated by the preliminary Au ion adsorption studies performed in this work, the high textural porosity of perturbed MSU silica, combined with their monodisperse microspherical morphology and uniform pore channel structure, opens up opportunities to generate nanoporous adsorbents and catalysts with both rapid and controlled diffusion properties (e.g., improving access and diffusion rates of reactive guests to the functional sites in the mesostructures). The ability to adjust the particle size of the mesostructures by adjusting cationic group loading represents another potentially useful feature of this synthesis route. The results of these ion adsorption studies confirm the findings observed by previous work done in ion adsorption, namely that uniform nanoporosity promotes optimal access of ions to ligand groups incorporated within the pore channels of mesostructured silicas, whereas increasing disorder in the pore channels results in reduced adsorption capacity and poorer uptake kinetics.[7−9] The results, however, also show that the introduction of a small degree of disorder in the mesostructures, although not enough to significantly perturb the uniformity of the pore channels, imparts optimized adsorption capacity and uptake kinetics compared to mesostructures completely devoid of any morphological defects.

This report offers yet another tool in the ever-evolving arsenal of synthesis methodologies leading to the preparation of tailored nanostructured materials with controlled structural and functional characteristics.

Acknowledgment. We acknowledge the Natural Science and Engineering Council of Canada (NSERC) for funding, and the Ontario Graduate Scholarship Program for providing a graduate scholarship to LB.

Supporting Information Available: Figures S1−S6. This material is available free of charge via the Internet at http://pubs.acs.org.